LIMNOLOGY
and
OCEANOGRAPHY: METHODS

ASLO

Limnol. Oceanogr.: Methods 2021

doi: 10.1002/lom3.10473

A novel device for trace metal-clean sampling of bottom water and suspended particles at the ocean's lower boundary: The Benthic Trace Profiler

Anna Plass, Anna-Kathrin Retschko, Matthias Türk, Tim Fischer, Florian Scholz*
GEOMAR Helmholtz Centre for Ocean Research Kiel, Kiel, Germany

Abstract

The benthic boundary layer plays a crucial role in the exchange of trace metals between surface sediments and the water column. So far it has been difficult to study dissolved–particulate interactions of trace metals in this highly reactive interface layer due to the lack of suitable sampling methods. We developed a new device, called Benthic Trace Profiler (BTP), which enables simultaneous sampling of near-bottom water and suspended particles in high depth resolution within the first 3 m above the seafloor. The device was tested successfully in the Baltic Sea. The concentrations of several trace metals (Co, Ni, Cu, Zn, and Cd) in the collected bottom waters overlapped with concentrations in water column samples above collected with conventional methods. This observation indicates that the sampling device and method is trace metal clean. The trace metals Fe and Mn showed concentration gradients within the benthic boundary layer indicating an upward diffusive flux. This observation is consistent with a diffusive benthic flux of these trace metals across the sediment–water interface, which was independently verified using pore-water profiles. Suspended particles can be used to study precipitation processes and to determine the carrier phases of trace metals. The BTP fulfilled all the intended requirements as it allowed a simultaneous, uncontaminating and oxygen-free sampling of seawater and suspended particles to gather high-resolution profiles of dissolved and particulate trace metal concentrations above the seafloor. The device closes the gap between water column and sediment sampling and helps researchers to better understand trace metal exchange processes across the ocean's lower boundary.

Several trace metals (TMs) are essential micronutrients required for marine life. They are part of many enzymes, which catalyze important biological functions such as photosynthesis (Fe, Mn, and Cu) and carbon fixation (Co, Zn, and Cd). Because of generally low concentrations in the surface ocean the availability of TMs can regulate and (co-)limit primary productivity (Morel 2003; Saito et al. 2008; Moore et al. 2013; Morel et al. 2014; Lohan and Tagliabue 2018). Furthermore, sedimentary TM signatures can be used as proxies to infer marine biogeochemical cycling and redox conditions in the geological past (Brumsack 2006; Tribovillard et al. 2006; Sweere et al. 2016; Scholz 2018; Algeo and Liu 2020).

Trace metal fluxes across the sediment–water interface at ocean boundaries play an important role in regulating oceanic TM concentrations. In particular, sediments underlying oxygen minimum zones are a source for Fe, Mn, and Co and a sink for Ni, Cu, Zn, and Cd (Brumsack 2006; Böning et al. 2009; Little et al. 2015; Plass et al. 2021). However, the processes that are involved in benthic TM cycling are not fully understood. The benthic boundary layer may play a key role in modulating TM fluxes. This layer is characterized by high rates of chemical reactivity and exchange of dissolved and particulate matter between the water column and the seafloor (Boudreau and Jorgensen 2001). Depending on the prevailing redox conditions, TM precipitation can take place. For example, when dissolved Mn is released from anoxic sediments, it can reprecipitate in the bottom water through oxidation processes and therefore be returned to the sediment (Sundby and Silverberg 1985; Pakhomova et al. 2007). Similarly, after release from the sediments reduced Fe can be oxidized to poorly soluble Fe(III) by oxygen, nitrate, or nitrite (Scholz et al. 2016; Heller et al. 2017; Schlosser et al. 2018). Furthermore, when hydrogen sulfide escapes the sediment, TM removal from bottom water through sulfide precipitation can take place (especially CdS, which has a low solubility) (Jacobs et al. 1985; Sundby et al. 1986; Plass et al. 2020). Sampling of suspended particles at the benthic boundary is required to constrain these precipitation reactions and also to determine

*Correspondence: fscholz@geomar.de

by which carrier phase TMs are delivered from the water column to the sediment surface. The respective importance of different carrier phases is in many cases poorly constrained. For example, TM sequestration by phytoplankton and delivery with fresh organic material, TM scavenging by inorganic particles (e.g., metal oxides) or refractory organic material, and TM sulfide precipitation can contribute to the particulate supply of TMs to the sediment (Böning et al. 2004; Audry et al. 2006; Rigaud et al. 2013; Little et al. 2015; Ciscato et al. 2018). Furthermore, the biogeochemical conditions leading to TM precipitation in near-bottom waters need to be evaluated in order to gain further insights into benthic TM cycling and fluxes. This can ultimately help to better constrain the oceanic mass balances of TMs and to predict how environmental conditions impact the availability of TMs to marine organisms in the surface ocean.

Devices and procedures for TM sampling of the water column are well established, in particular by the GEOTRACES program (Scor Working Group 2007; Cutter and Bruland 2012), but fail in the benthic boundary layer. The conventional sampling methods by GO-FLO bottles cannot reach close enough to the seafloor. These bottles are commonly lowered only to a maximum depth of 5 m above the seafloor to avoid damage to and contamination of the bottle by touching the seafloor and sampling of artificially resuspended particles. Furthermore, as GO-FLO bottles are lowered vertically, the samples represent an integrated signal over the height of the bottle (typically > 1 m), which is an unsatisfying vertical resolution close to the seafloor. On the other hand, sampling of seawater right above the seafloor is often conducted by the aid of a multiple corer and by collecting the water overlying the sediment (~ 20–30 cm) or by attaching a Niskin bottle to the frame of a multiple corer. By this method, only a single sample representing the first few centimeters to decimeters or meter above the seafloor can be collected. Furthermore, resuspension of sediments to the bottom water or admixing of oxygen during core retrieval and recovery can lead to mixing of pore water and bottom water and/or artificial TM scavenging. With both methods mentioned, it is not possible to capture concentration gradients in the first few meters above the seafloor.

To close the gap between water column and sediment sampling, bottom water samplers (e.g., K.U.M., MARUM) and benthic landers or vehicles equipped with sampling bottles (Guo and Santschi 2000) or peristaltic pumps and syringes (Holtappels et al. 2011) have been developed. However, these instruments consist of a metal frame (or contain metal parts) and/or are equipped with Niskin bottles with metal springs in the interior. Therefore, these instruments are well suited for sampling of nutrients or organic compounds but do not meet the requirements for contamination-free TM sampling. In addition, the sampling bottles are open while the devices are lowered to the seafloor so that resuspended particles rather than naturally suspended particles are collected upon placement at the seafloor. Furthermore, not all sampling bottles are suited for in-line filtration under oxygen free conditions or particle sampling.

To overcome these problems a team of engineers and scientists designed and custom-built a new device, which fulfills the following requirements:

1. Close the gap between water column and sediment sampling.
2. Simultaneous sampling of suspended particles and seawater in the benthic boundary layer.
3. Sampling at several adjustable depths above the seafloor to resolve vertical gradients.
4. Sampling with a low risk of contamination.
5. Sampling under oxygen-free and/or in situ redox conditions.

Use materials and procedures

Sampling site

The Benthic Trace Profiler (BTP) was tested successfully during two short cruises of RV *Alkor* in October 2018 and March 2019. Our sampling location Boknis Eck (54°31.2′N, 10°02.5′E) has a water depth of around 30 m and is located in the southwestern Baltic Sea at the entrance of Eckernförde Bay (Fig. 1). Boknis Eck is a time series station, which has been studied and sampled by marine scientists in Kiel for more than 60 yr. The site is monitored on a regular basis for physical and chemical water column properties such as temperature, salinity, oxygen, dissolved nutrients, and chlorophyll (*see* https://

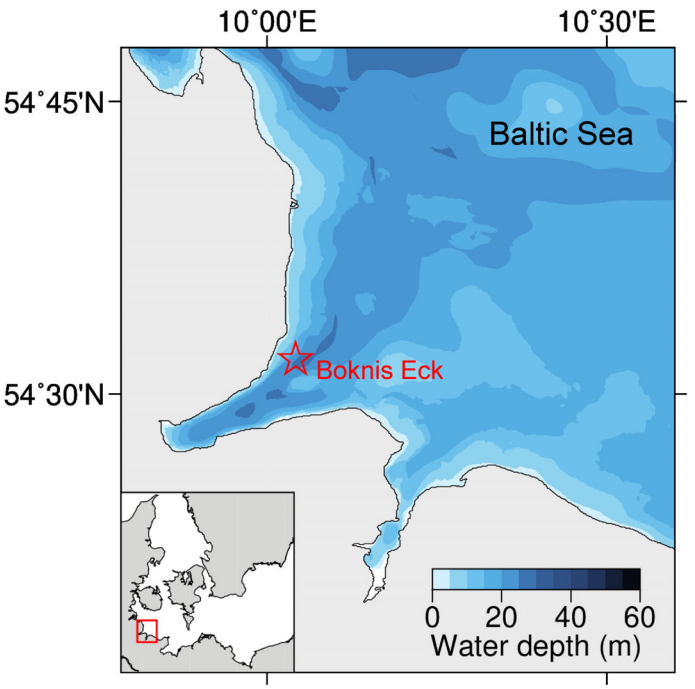

Fig 1. Sampling site Boknis Eck in the southwestern Baltic Sea.

www.bokniseck.de/de/home for data). A strong seasonal variability of the biogeochemical conditions in the water column is characteristic for this site. The seasonal phytoplankton bloom in spring is accompanied by intense export production of organic material. Seasonal stratification during summer and early fall together with organic matter respiration leads to oxygen depletion culminating occasionally in the occurrence of sulfidic conditions within the deepest water layers at Boknis Eck (within few meters above the sediment). In contrast, during the winter period, the water column is generally well ventilated and fully oxygenated (Smetacek 1980; Hansen et al. 1999; Bange et al. 2011; Lennartz et al. 2014). Due to the seasonal changes in oxygen and redox conditions, Boknis Eck is well suited to study how these different biogeochemical conditions impact TM cycling within the benthic boundary layer. Moreover, since the seafloor at Boknis Eck is located within a local bathymetric depression with a seasonally stratified water column and strongly reducing conditions in the sediment, concentration gradients within the near-bottom waters are likely to be established.

Sampling system and operating mode

All the individual features of the novel bottom water sampler, described in the following paragraphs, are displayed in technical drawings in Fig. 2. The BTP consists of a titanium frame with a height of roughly 3 m. Five modified GO-FLO bottles (General Oceanics) with a volume of 2.5 liters each are attached horizontally to the frame at adjustable depths (default is 0.3, 0.9, 1.5, 2, and 2.6 m above the seafloor). The sampling depths can be adjusted to the expected thickness of the benthic boundary layer and concentration gradients. During our test cruises, we intended to sample the transition between the seafloor, which can be sampled using a multiple corer, and the open water column, which can be sampled by conventional sampling bottles. The main goal was to evaluate whether our approach is TM clean and capable of resolving TM concentration gradients within this transition zone. The heights of the GO-FLO bottles above the seafloor was chosen accordingly, that is, minimal and maximal possible distance from the seafloor to prevent penetration of the lowermost bottle in the sediment and minimize the distance between the BTP and water column profiles.

The sampling bottles are equipped with a plastic gear to their opening mechanism (Fig. 3). The gear on the bottles is attached to a gear transmission on the frame, which is controlled by a programmable electric motor (K.U.M. Umwelt- und Meerestechnik Kiel GmbH) that steers the opening and closing of the sampling bottles. The motor is powered by a battery pack (24 x Emmerich NiMH-Akku SUB-C 4000mAh ZLF) within a deep-sea certified pressure housing. Before the sampling bottles are attached to the device, they are filled with deionized water (Milli-Q, Millipore) and closed manually to avoid implosion due to the increasing hydrostatic pressure under water. The device is then lowered to the seafloor using the winch and wire of a research vessel. The Profiler is connected to the wire with a swivel shackle and equipped with a fin allowing it to align with the prevailing current. Floats are attached to the wire above the instruments to prevent it from entangling in the BTP. The bottom weights (24×14 kg) that promote the sinking of the Profiler through the water column are coated with plastic to preclude metal contamination. A bottom plate prevents the profiler from sinking into the sediment. Once placed on the seafloor, a bottom contact sensor is triggered and after a programmed period of time (e.g., 15 min) the sampling bottles are opened by the electric motor and gear transmission. The delay between the placement of the device and the opening of the bottles allows particles that were resuspended to settle down and/or to be transported away by currents. Once the bottles are opened, the deionized water is replaced by denser (saline) near-bottom water including naturally suspended particles. After another programmed period of time (e.g., 5 min), the bottles are closed again and the device is raised back to the ship's deck. As an alternative to the automatic opening and closing mechanism, the deployment can also be monitored visually and remotely controlled using a deep-sea telemetry. Visual observation during some test deployments suggested that 15 min are sufficient to let resuspended particles disappear. In addition, it is planned to equip the BTP with a transmissometer in order to be able to monitor particle concentrations over the deployment time. After recovery, the sampling bottles are detached from the frame and taken to the lab, where they are attached to a custom-built rack (Fig. 3).

The following sampling procedure corresponds to GEOTRACES standards (Cutter et al. 2010) and recommendations by Planquette and Sherrell (2012). An inert gas line (argon) is connected to the bottles pressure valve. The gas creates an overpressure (~ 0.2 bar) to collect the water samples and particles under oxygen-free conditions through the sampling spigot. During our test cruises, suspended particles were collected on 0.2 μm polyether sulfone filters (Supor, diameter 47 mm). The near-bottom water was collected in 250 mL low-density polyethylene (LDPE) bottles. Salinity was measured on each near-bottom water sample to assure that the deionized water in the sampling bottles was replaced completely by ambient seawater. The near-bottom water was acidified to a pH < 2 with subboiling distilled HNO_3. After the near-bottom water was sampled ($\sim$ 1 h after recovery of the BTP), the filter holder was immediately transferred into a glove bag filled with argon to prevent oxidation reactions. Inside the glove bag, the filter holders were opened and the filters containing the suspended particles were collected and stored in Analyslides (Pall Laboratory). Subsequently, the filters were vacuum sealed and frozen until total digestion or sequential extraction followed by TM analyses or synchrotron radiation-based X-ray analyses. These solid phase analysis and the corresponding interpretation are not the focus of this manuscript and will be presented in a separate publication. All materials used for

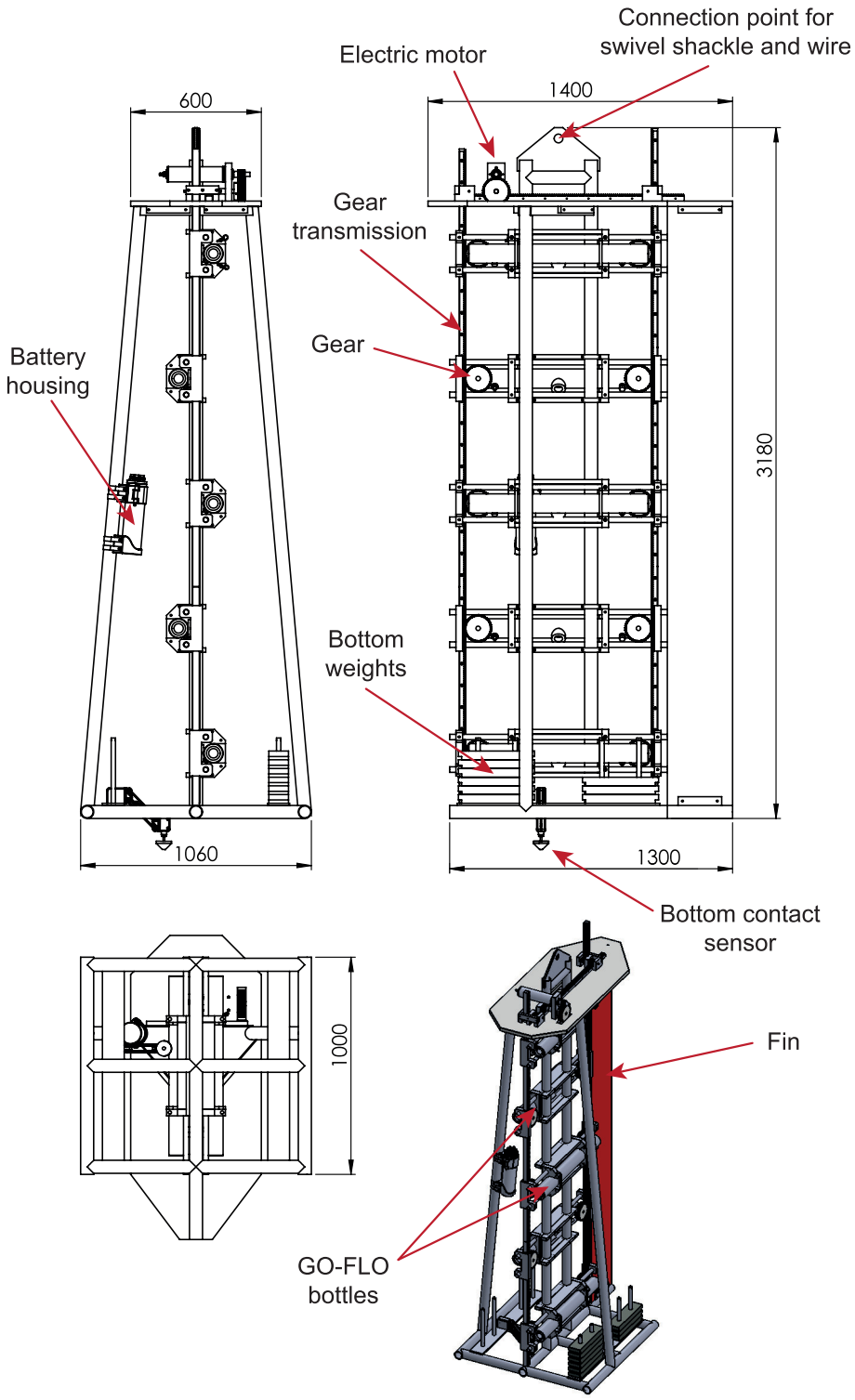

Fig 2. Technical drawing of the BTP. The different views are displayed to visualize the individual features of the Profiler (upper left: side view; upper right: front view; lower left: top view; lower right: trimetric view). Numbers indicate dimensions in millimeters.

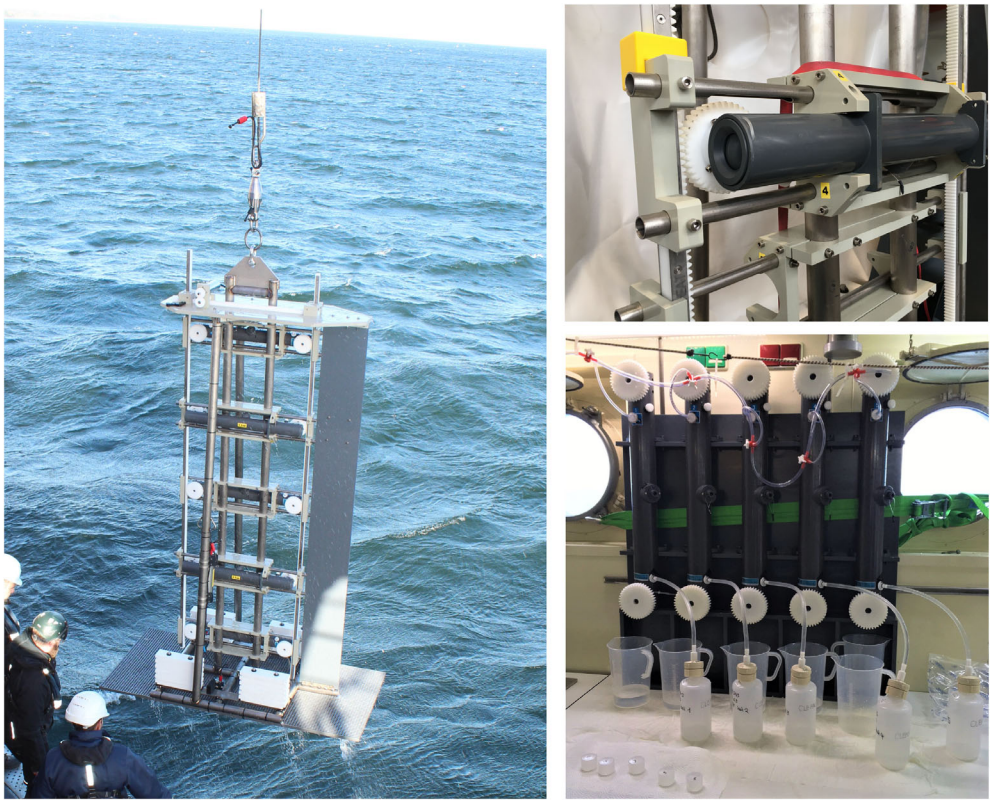

Fig 3. BTP during deployment in the Baltic Sea (left); close-up of modified sampling bottle and gear transmission mechanism (upper right); in-line filtration of samples in the ship's lab (lower right).

sampling (sample bottles, tubing and filters) were acid cleaned and rinsed thoroughly with deionized water before usage following GEOTRACES standards (Cutter et al. 2010).

Ancillary sampling and measurements

General water column properties such as temperature, salinity, and oxygen concentrations were determined using a CTD sensor system. To test the TM concentration results obtained by our new sampling method, we additionally took water column samples using a conventional TM clean sampling method following the GEOTRACES protocol (Cutter et al. 2010). For this purpose, GO-FLO bottles were clamped to a noncontaminating cable, lowered through the water column and triggered with messengers at five depths (5, 10, 15, 20, and 25 m). The GO-FLO bottles were always deployed before the BTP ($\sim$ 30 min) to avoid water column contamination due to sediment trailing off the sampler's bottom plate on recovery (which could create an artificial match between results from the two sampling systems). In the ship's laboratory, the collected water column samples were processed identically to bottom water samples: an inert gas line (argon) was attached to create an overpressure (0.2 bar) and the water sample was collected in LDPE bottles and acidified to a pH < 2 with subboiling distilled HNO_3.

To identify and quantify benthic diffusive TM fluxes across the sediment–water interface, we took short sediment cores ($\sim$ 30 cm depth with overlying bottom water) with a multiple corer. The overlying bottom water was collected and filtered through 0.2 μm cellulose acetate syringe filters (Sartorius) immediately after retrieval. The core was then transferred to a glove bag filled with argon and sliced into depth intervals. These samples were then centrifuged to separate solid sediment and pore water. The supernatant pore water was filtered in another argon filled glove bag and transferred to acid cleaned LDPE bottles. Pore-water and supernatant bottom water samples were acidified to pH < 1 with subboiling distilled HNO_3. Separate nonacidified pore-water samples were used to measure hydrogen sulfide concentrations (U-2001 Hitachi spectrometer) using a standard photometric technique (Grasshoff et al. 1999). Additional uncentrifuged sediment samples were collected in preweighed plastic cups to determine water content and porosity.

An estimate for the turbulent eddy diffusivity (D_T) within the benthic boundary layer was derived from another campaign in September 2018, which took place in the area of Boknis Eck. During the Baltic Sea Gas Exchange Experiment (RV *Alkor* cruise Al516), a microstructure probe (MSS 90L of Sea & Sun Technology) was deployed from a small boat obtaining full depth profiles of microstructure velocity shear at 17 stations with three profiles each. The MSS was equipped

with two airfoil shear sensors and standard CTD sensors. Seven of the stations were deep enough (> 23 m) to show a benthic boundary layer consistent with that seen in October 2018 and March 2019 at Boknis Eck. The measured microstructure velocity shear within the benthic boundary layer was used to estimate the turbulent dissipation rate (Oakey 1982), which subsequently is the base to estimate the diapycnal diffusivity (Osborn 1980), that is, the turbulent eddy diffusivity perpendicular to density isolines. Further details on microstructure data processing and calculations may be found in Fischer et al. (2013).

TM analysis

For TM analysis of water column and near-bottom water samples, we followed a preconcentration method using an automated preconcentration device (SeaFAST) (Rapp et al. 2017). Briefly, a 15 mL sample was pH-buffered to 6.4 with an ammonium acetate buffer (1.5 M) before it was loaded onto a chelating resin column where the seawater matrix was rinsed off. The TMs were then collected by eluting the column with acid (1 M subboiling distilled HNO_3). For the preconcentration of TMs from pore-water samples, we followed the same procedure but with a half-automated device (Preplab), due to the lower volume of sample available. For this method, 1 mL of pore water was required and the buffer addition and sample loading was conducted manually.

The preconcentrated samples were analyzed by high resolution inductively coupled plasma mass spectrometry (HR-ICP-MS; Thermo Fisher Element XR). TM concentrations were quantified by standard addition (Mn, Co) and isotope dilution (Ni, Cu, Zn, and Cd). Accuracies and detection limits of this method are listed in Plass et al. (2020, 2021). The analytical error was determined through error propagation of the standard deviation from replicate measurements of samples and standards.

Diffusive flux calculations

The diffusive fluxes (F_D) of Fe and Mn across the sediment–water interface were determined by Fick's first law of diffusion:

$$F_D = -\phi D_{sed}\left(\frac{dC}{dx}\right) \quad (1)$$

In this equation, ϕ represents porosity and dC/dx is the concentration difference between the uppermost pore-water sample (0–1 cm sediment depth) and the lowermost GO-FLO bottle of the BTP. We assume that TM concentrations in the lowermost GO-FLO bottle provide a better estimate of the TM concentrations immediately above the seafloor than bottom waters overlying the sediment in multiple corer tubes (*see* the introductory paragraphs). The effective molecular diffusion coefficient of a TM in the sediment (D_{sed}) was derived from the diffusion coefficients in seawater (D_{sw}) under standard conditions (Li and Gregory 1974) and adjusted to in situ temperature, pressure and salinity by applying the Stokes–Einstein equation and by dividing by tortuosity (Boudreau 1997):

$$D_{sed} = D_{sw}/\left(1 - \ln\left(\phi^2\right)\right) \quad (2)$$

A negative flux is directed from the pore water into the bottom water. All input data and diffusive fluxes are listed in Table 1.

In analogy to the diffusive benthic flux across the sediment–water interface, the turbulent flux across the benthic boundary layer was calculated as follows:

$$F_T = -D_T\left(\frac{dC}{dx}\right) \quad (3)$$

In this equation, D_T is the turbulent eddy diffusivity and dC/dx is the vertical concentration gradient over the depth range sampled by the BTP.

Assessment

During our two sampling campaigns, we observed differing physicochemical conditions in the water column (Fig. 4) and differing concentration gradients of hydrogen sulfide in the surface sediment (Fig. 5). In October 2018, the water column was more stratified and the deep water was characterized by lower oxygen concentrations (130 μM O_2) compared to the cruise in March 2019 (250 μM O_2). The surface sediment was highly sulfidic during October when hydrogen sulfide concentrations reached up to 3 mM within the first few centimeters

Table 1. Input data for diffusive flux calculations and diffusive fluxes of iron and manganese.

Element	Sampling season	Bottom water concentration* (μM)	Concentration at sediment surface (μM)	Porosity	Effective molecular diffusion coefficient ($cm^2\ s^{-1}$)	Diffusive flux ($mmol\ m^{-2}\ yr^{-1}$)
Fe	Oct	0.018	1.33	0.94	4.37×10^{-6}	−3.4
Fe	Mar	0.026	25.08	0.93	3.22×10^{-6}	−47.3
Mn	Oct	0.204	18.24	0.94	4.26×10^{-6}	−45.8
Mn	Mar	0.007	21.22	0.93	3.14×10^{-6}	−39.0

*Measured in the lowermost GO-FLO bottle of the BTP.

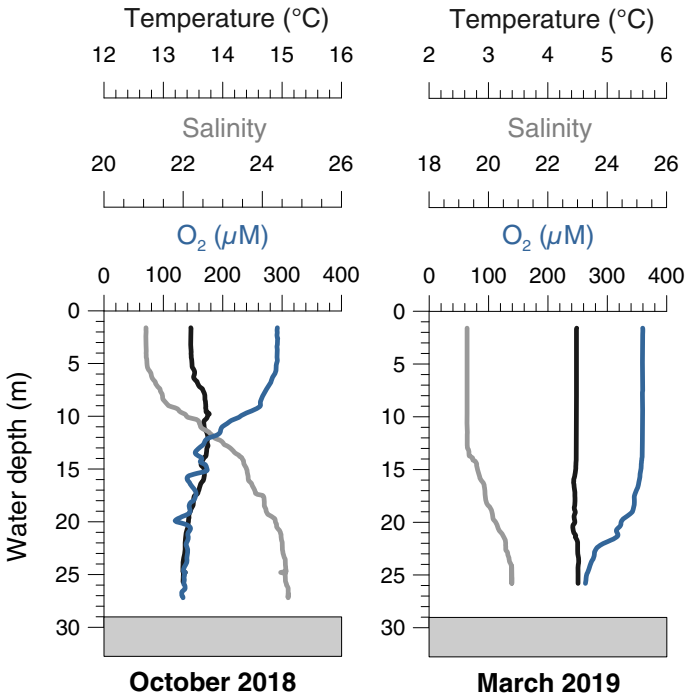

Fig 4. Water column temperature, salinity, and oxygen profiles during the sampling campaigns in October 2018 (left) and March 2019 (right) at Boknis Eck. The gray shaded area represents the seafloor.

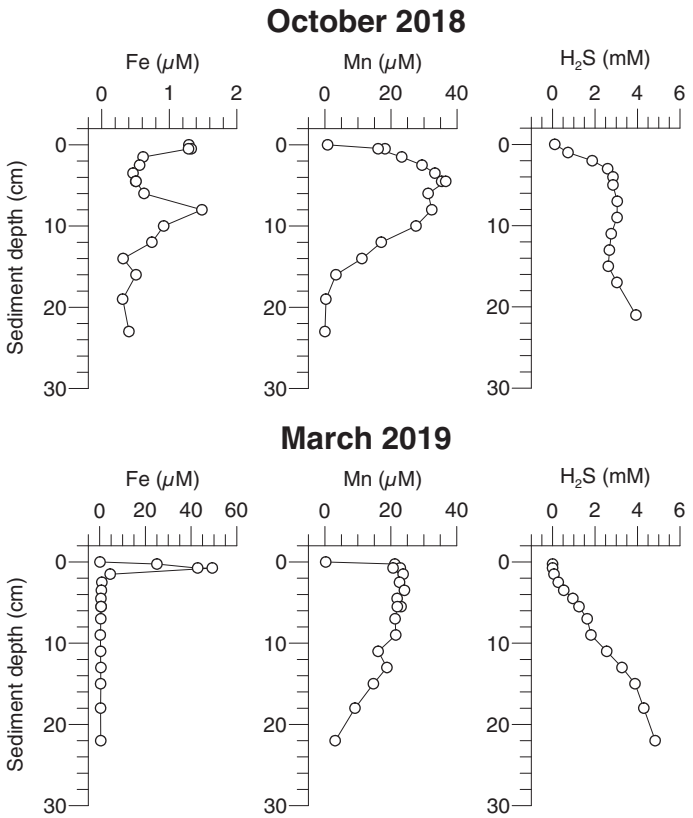

Fig 5. Pore-water concentrations of Fe, Mn, and hydrogen sulfide during the sampling campaigns in October 2018 (upper panel) and March 2019 (lower panel). The uppermost point of each profile represents bottom waters sampled with the multiple corers. Note differing axes scales for Fe.

of the sediment core. In contrast, during the March campaign, no hydrogen sulfide was present at the sediment surface and H_2S concentrations remained below 1 mM within the first few centimeters of the sediment core. As the mobility and cycling of TMs is dependent on redox conditions (Sundby et al. 1986; Morford and Emerson 1999; Tribovillard et al. 2006; Scholz and Neumann 2007; Scholz et al. 2011; Rigaud et al. 2013; Rapp et al. 2020), the differing redox-conditions during our test deployments are expected to affect TM gradients close to the seafloor.

Comparison of TM concentrations in near-bottom water and water column samples

To identify potential contamination of samples obtained by our new sampling device, we compared TM concentrations in samples taken with the BTP to concentrations in water column samples taken above with GO-FLO bottles according to the widely applied GEOTRACES protocol. The concentrations show some variability as a function of water depth and season (Fig. 6). However, in general, there is a good agreement between concentrations obtained by the two different sampling methods. With the exception of one sample in the Fe profile of the March campaign (Fig. 6b), TM concentrations in near-bottom waters are generally consistent with the range of concentrations observed in the water column above (Table 2). Most notably, the concentrations of Zn, a TM that is highly prone to contamination (Cutter and Bruland 2012), matched well with water column concentrations. Given the generally consistent concentration range in the open water column and near-bottom water, we see no evidence for contamination.

TM concentrations in the water column were variable between sampling campaigns. This seasonal concentration change was also reflected in near-bottom water samples collected with the BTP. During October, the concentrations of Ni, Cu, Zn, and Cd were around half or less than half compared to the March campaign. This observation could be related to enhanced TM sequestration by phytoplankton and organic material during and after the productive season (Sundby et al. 1986; Kremling et al. 1997; Brügmann et al. 1998; Pohl and Hennings 2005; Bruland and Lohan 2006; Scholz et al. 2011; Noble et al. 2012; Rigaud et al. 2013; Rapp et al. 2019). In addition, more reducing and sulfidic conditions in the bottom water and/or sediment before/during the October campaign may have led to TM removal into sulfide minerals (Sundby et al. 1986; Brügmann et al. 1998; Pohl and Hennings 2005; Rigaud et al. 2013).

Some near-bottom water samples were characterized by elevated concentrations of Co (March), Zn, and Cd (both March and October) relative to the water column above, but without clear depth trend toward the seafloor. This observation could

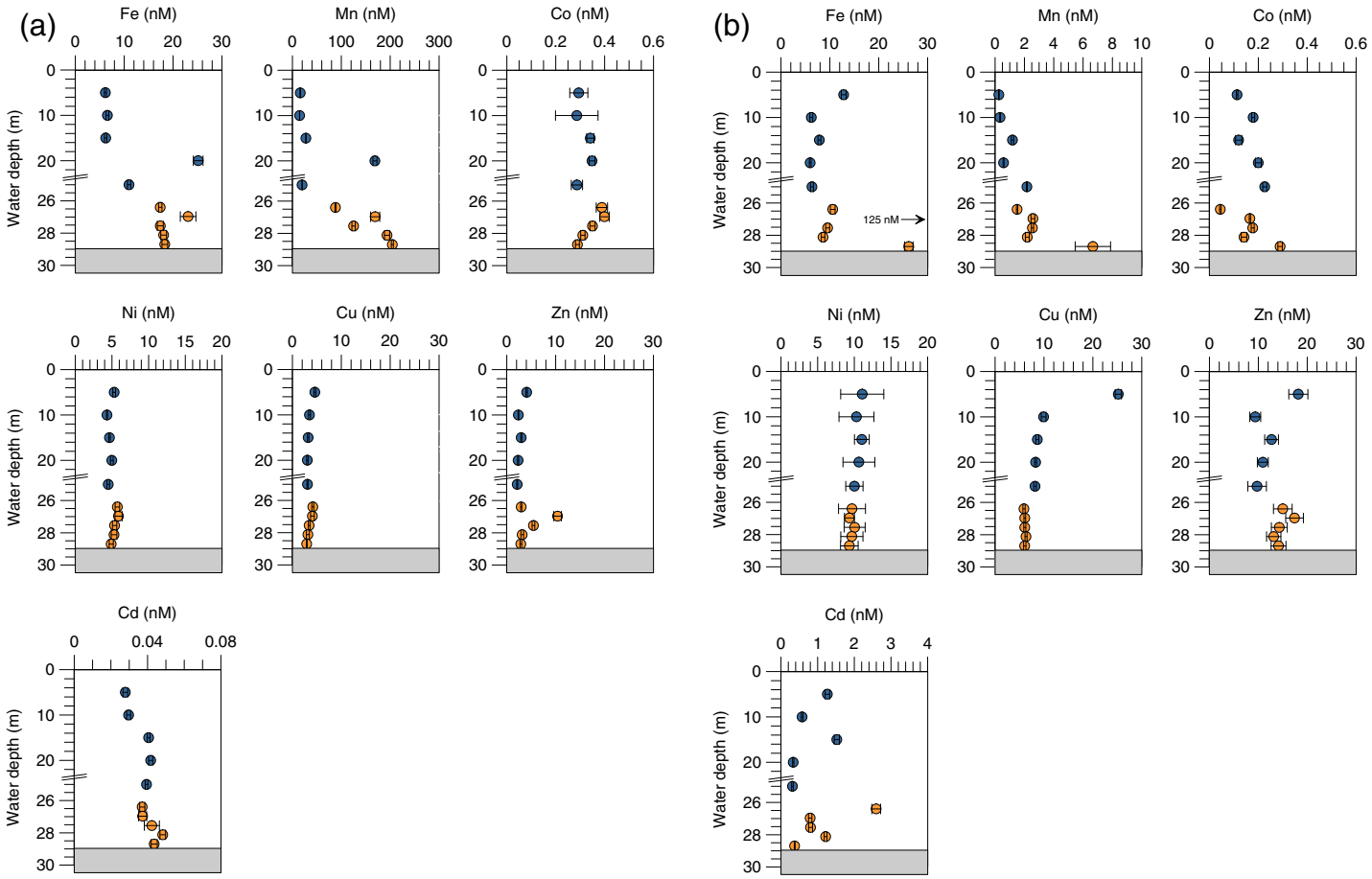

Fig 6. Dissolved (< 0.2 μm) trace metal concentrations in the water column (blue) and near-bottom water (orange) at Boknis Eck during the sampling campaign in October 2018 (**a**) and March 2019 (**b**). The analytical errors derived by error propagation are shown as black bars. The gray shaded area represents the seafloor. Note differing axes scales for Mn and Cd in (**a**) and (**b**).

Table 2. Concentration range of trace metals within the water column and within near-bottom waters.

	Oct		Mar	
	Water column	**Bottom water**	**Water column**	**Bottom water**
Fe (nM)	6.2–25.1	17.4–23.1	6.2–12.8	8.6–26.1 (125)
Mn (nM)	14.7–168.7	88.0–204.4	0.26–2.2	1.5–6.7
Co (nM)	0.29–0.45	0.29–0.40	0.11–0.23	0.04–0.29
Ni (nM)	4.3–5.3	4.9–5.9	10.0–11.0	9.3–10.0
Cu (nM)	3.1–4.6	2.9–4.2	8.2–25.2	5.9–6.3
Zn (nM)	2.1–4.1	2.9–10.4	9.4–18.2	14.1–17.4
Cd (nM)	0.28–0.42	0.37–0.48	0.31–1.52	0.37–2.60

be related to TM release from organic-rich particles within the benthic boundary layer (Scholz and Neumann 2007; Plass et al. 2021). Highly elevated and increasing concentrations toward the seafloor were observed for Fe and Mn. This type of profile is indicative of a sedimentary source of these elements at our study site (*see following* Section). Concentration maxima of Fe and Mn at 20 m water depth during the October campaign (Fig. 6a) could be related to lateral supply from anoxic sediments surrounding the bathymetric depression of Boknis Eck.

Comparison of concentration gradients in near-bottom waters to benthic fluxes

The BTP was designed to detect TM concentration gradients within the benthic boundary layer. In particular, Mn showed

a clear concentration gradient within the near-bottom waters during the October campaign. The concentration of Mn increased almost linearly from 88.0 to 204 nM within the water layer sampled by the BTP. During March, only the sample from immediately above the seafloor (0.3 m) was characterized by elevated Mn (6.7 nM) and Fe (26.1 nM) concentrations compared to the overlying water column (Mn: 1.5 nM, Fe: 8.5 nM). The distance over which Mn and Fe concentrations in bottom water decline can be explained by differing oxygen concentrations in the bottom water during the two campaigns. Under more reducing conditions in October, Mn and Fe concentrations decrease more steadily over the 3 m sampled by the BTP (Fig. 6a), which may be related to slower oxidation kinetics at lower oxygen concentrations (Fig. 4) (Millero et al. 1987; von Langen et al. 1997). By contrast, under more oxygenated conditions in March, Mn and Fe oxidation take place more rapidly, which is why the positive concentration anomaly is limited to the lowermost BTP sample (Fig. 6b). The differing Fe gradients in October and March suggest that no oxygen contamination took place during sampling as this would have resulted in rapid Fe oxidation and precipitation as Fe (oxyhydr)oxide.

The trend of differing Mn and Fe concentrations in near-bottom water during our two test cruises is consistent with the temporal evolution of pore-water profiles and diffusive benthic fluxes. The pore-water profiles of Mn and Fe (Fig. 5) show downward increasing concentrations across the sediment–water interface, which is indicative of a sedimentary Mn and Fe efflux (Table 1). The diffusive benthic Mn flux was about equal in October and March (October 2018: -46 mmol m^{-2} yr^{-1}, March 2019: -39 mmol m^{-2} yr^{-1}). By contrast, the diffusive benthic flux of Fe was higher during March, when the conditions were overall less reducing (October: -3.4 mmol m^{-2} yr^{-1}, March -47 mmol m^{-2} yr^{-1}). This opposing trend can be explained by the differing tendency of Fe and Mn to form sulfide minerals. Manganese is relatively mobile under anoxic-sulfidic conditions. By contrast, Fe is precipitated as Fe monosulfide (FeS) and subsequently converted to pyrite (FeS_2) under anoxic-sulfidic conditions (Berner 1970; Rickard and Morse 2005). Since Fe concentrations in sulfidic pore water are limited to < 1 μM (Rickard 2006), the diffusive benthic Fe flux decreases upon transition from anoxic-ferruginous (Fe-rich) to sulfidic conditions within the surface sediment (Scholz et al. 2014).

Provided that the turbulent eddy diffusivity in the benthic boundary layer is known, the TM gradients obtained with the BTP can be used to estimate vertical diffusive fluxes. These flux estimates can then be compared to other components of the TM budget within the benthic boundary layer, for example, the sediment efflux. As an example, we use the Mn gradient observed during the October campaign (Fig. 6a) combined with an estimate of the turbulent eddy diffusivity to quantify vertical diffusive Mn transport across the benthic boundary layer. As there was no simultaneous measurement of turbulent eddy diffusivity during the BTP deployment, we use an estimate for D_T in the benthic boundary layer, which is derived from microstructure measurements conducted nearby in September 2018 (*see Method* Section). The seven microstructure stations selected show a close hydrographic similarity to the October 2018 CTD profile, particularly in the stratification in the benthic boundary layer, which varies from $N^2 = 0.7 \times 10^{-4}$ s^{-2} to $N^2 = 7.8 \times 10^{-4}$ s^{-2} in September vs. a value of $N^2 = 2 \times 10^{-4}$ s^{-2} in October. Above the benthic boundary layer of 1.5–4 m thickness lies the strongly stratified water column with N^2 at least an order of magnitude larger than below. The corresponding values for D_T vary between 0.1×10^{-4} m^2 s^{-1} and 5×10^{-4} m^2 s^{-1} for the benthic boundary layer, with an average of 1.3×10^{-4} m^2 s^{-1}. Above the benthic boundary layer D_T reduces distinctly to values between 10^{-6} and 10^{-5} m^2 s^{-1}. Assuming that the hydrographic similarity implies similar diffusive mixing, we may estimate D_T within the benthic boundary layer to be of the order of 10^{-4} m^2 s^{-1}. The uncertainty of this estimate is rather high and may be on the order of factor 10, as mixing estimates from microstructure profiles usually have uncertainties of factor two, plus taking into account the variability of D_T found in September 2018, and the uncertainty how comparable the regimes in September and October really are.

Adopting a D_T of 10^{-4} m^2 s^{-1} and dC/dx of 40 μmol m^{-4} yields an upward directed Mn flux of -126 mmol m^{-2} yr^{-1}. Considering the large uncertainties that are associated with the methods applied (eddy diffusivity and concentration gradient across the sediment–water interface), we note that this estimate is generally of the same order of magnitude as the diffusive benthic Mn efflux (-46 mmol m^{-2} yr^{-1}) (Table 1). This observation confirms that sedimentary Mn release and transport across the benthic boundary layer are connected. However, the uncertainties of the two flux estimates are too high to estimate other components of the budget like Mn removal rates. During future campaigns, microstructure measurements should be conducted during the BTP deployment. Such an approach could be used to determine how much of the sediment-derived TMs can be transported across the benthic boundary layer into the open water column.

Previous studies on oxygen transport within the benthic boundary layer revealed that current dynamics play an important role in modulating sedimentary oxygen uptake in dynamic seafloor environments (Koopmans et al. 2021; Reimers and Fogaren 2021). Physical measurements over multiple BTP deployments may help to evaluate if variable currents and the associated oxygen dynamics affect TM transport and removal within the benthic boundary layer.

Discussion

Our results demonstrate that the BTP is well suited for the sampling of TMs that are prone to contamination. The sampling height and distances are suited to detect changes in

concentration profiles within near-bottom waters. Furthermore, the height of the sampling bottles above the seafloor is variable and can be adjusted to the requirements of the respective seafloor environment or study.

During our test cruises, we were able to detect elevated TM concentrations close to the seafloor (0.3 m) using the BTP. A water column sampling campaign based on GO-FLO bottles alone would have failed to detect these gradients, because these sampling devices cannot be lowered this close to the seafloor, thus leaving a blind spot at the benthic boundary. On the other hand, when elevated concentrations in bottom waters above the seafloor are derived from measurements of bottom water overlying sediment cores, it is uncertain whether these are natural or due to mixing of pore water and bottom water during core retrieval and recovery. In addition, it is unclear whether elevated concentrations persist at greater distance from the seafloor as revealed here for Mn during the October campaign using the BTP. In more general terms, our observations underscore that near-bottom waters are an important transitional environment where TM fluxes from the sediment are modulated and transmitted to the open water column. In future applications, the BTP should be accompanied by further simultaneous or near-simultaneous physical monitoring of the water column and of the benthic boundary layer. Velocity profiles could help characterize the benthic boundary layer, help estimate lag time before opening BTP bottles, and help estimate vertical shear and turbulent diffusivity near the bottom. When combining the BTP deployment with simultaneous microstructure measurements, it may be possible to determine vertical diffusive fluxes more precisely and decide whether concentration gradients derive from TM precipitation or simple dilution. In this context, it is important to note that the new sampling device can be used without contaminating samples with oxygen. Therefore, it is possible to detect natural concentration gradients that arise from redox-controlled TM precipitation within the near-bottom water.

As the BTP has no limit in deployment depth, it is not limited to deployment in coastal or shelf environments; it is also well-suited for deep-sea research, for example, in the context of studies on the impact of mining of Mn nodules or on sediment-hosted hydrothermal systems. Another potentially important field of application of the BTP is studies on the so-called boundary exchange of rare earth elements (REEs) (especially neodymium [Nd]). It has been suggested that marine sediments represent a major source of Nd to the ocean (Abbott et al. 2015a,b), which has implications for the applicability of Nd isotopes as a tracer for past ocean circulation. However, the processes by which Nd and other REEs are remobilized and how sedimentary fluxes affect water mass signatures are still poorly constrained (Haley et al. 2017). The BTP is a suitable tool to investigate how water mass and sedimentary REE and Nd isotope signatures are affected by benthic fluxes and interactions with suspended particles close to the seafloor.

Future benthic studies of dissolved TM concentrations (and isotopes) in combination with the analysis of suspended particles will give valuable information about TM fluxes, precipitation processes, and carrier phases. Combined with the evaluation of environmental conditions, this will help to better understand and quantify TMs cycling and fluxes at the ocean's lower boundary.

References

Abbott, A. N., B. A. Haley, and J. McManus. 2015a. Bottoms up: Sedimentary control of the deep North Pacific Ocean's ε Nd signature. Geology **43**: 1035. https://doi.org/10.1130/G37114.1

Abbott, A. N., B. A. Haley, J. McManus, and C. E. Reimers. 2015b. The sedimentary flux of dissolved rare earth elements to the ocean. Geochim. Cosmochim. Acta **154**: 186–200. doi:10.1016/j.gca.2015.01.010

Algeo, T. J., and J. Liu. 2020. A re-assessment of elemental proxies for paleoredox analysis. Chem. Geol. **540**: 119549. doi:10.1016/j.chemgeo.2020.119549

Audry, S., G. Blanc, J. Schäfer, G. Chaillou, and S. Robert. 2006. Early diagenesis of trace metals (Cd, Cu, Co, Ni, U, Mo, and V) in the freshwater reaches of a macrotidal estuary. Geochim. Cosmochim. Acta **70**: 2264–2282. https://linkinghub.elsevier.com/retrieve/pii/S0016703706000718

Bange, H. W., A. Dale, H. P. Hansen, J. Karstensen, F. Malien, C. Petereit, K. Laß, and G. Friederichs. 2011. LOICZ-affiliated activities Boknis Eck time series station (SW Baltic Sea): Measurements from 1957 to 2010. LOICZ Inprint **2011**: 16–22. https://oceanrep.geomar.de/12198/

Berner, R. A. 1970. Sedimentary pyrite formation. Am. J. Sci. **268**: 1–23.

Böning, P., H.-J. Brumsack, M. E. Böttcher, B. Schnetger, C. Kriete, J. Kallmeyer, and S. L. Borchers. 2004. Geochemistry of Peruvian near-surface sediments. Geochim. Cosmochim. Acta **68**: 4429–4451. https://linkinghub.elsevier.com/retrieve/pii/S001670370400403X

Böning, P., H.-J. Brumsack, B. Schnetger, and M. Grunwald. 2009. Trace element signatures of Chilean upwelling sediments at ~36°S. Mar. Geol. **259**: 112–121. doi:10.1016/j.margeo.2009.01.004

Boudreau, B. P. 1997. Diagenetic models and their implementation. Springer. http://www.ncbi.nlm.nih.gov/pubmed/1163368

Boudreau, B. P., and B. B. Jorgensen. 2001. The benthic boundary layer: Transport processes and biogeochemistry, v. **82**. Oxford Univ. Press, p. 658–658. doi:10.1029/01EO00381

Brügmann, L., R. Hallberg, C. Larsson, and A. Löffler. 1998. Trace metal speciation in sea and pore water of the Gotland Deep, Baltic Sea, 1994. Appl. Geochem. **13**: 359–368. https://linkinghub.elsevier.com/retrieve/pii/S0883292797001054

Bruland, K. W., and M. C. Lohan. 2006. Controls of trace metals in seawater, p. 23–47. *In* H. Elderfield [ed.], The oceans and marine geochemistry, treatise on geochemistry. Elsevier. https://linkinghub.elsevier.com/retrieve/pii/B9780080959757006021

Brumsack, H.-J. 2006. The trace metal content of recent organic carbon-rich sediments: Implications for Cretaceous black shale formation. Palaeogeogr. Palaeoclimatol. Palaeoecol. **232**: 344–361. https://linkinghub.elsevier.com/retrieve/pii/S0031018205002737

Ciscato, E. R., T. R. R. Bontognali, and D. Vance. 2018. Nickel and its isotopes in organic-rich sediments: Implications for oceanic budgets and a potential record of ancient seawater. Earth Planet. Sci. Lett. **494**: 239–250. doi:10.1016/j.epsl.2018.04.061

Cutter, G. A., and K. W. Bruland. 2012. Rapid and non-contaminating sampling system for trace elements in global ocean surveys. Limnol. Oceanogr.: Methods **10**: 425–436. doi:10.4319/lom.2012.10.425

Cutter, G. A., and others. 2010. Sampling and sample-handling protocols for GEOTRACES cruises. https://epic.awi.de/id/eprint/34484/

Fischer, T., D. Banyte, P. Brandt, M. Dengler, G. Krahmann, T. Tanhua, and M. Visbeck. 2013. Diapycnal oxygen supply to the tropical North Atlantic oxygen minimum zone. Biogeosciences **10**: 5079–5093. doi:10.5194/bg-10-5079-2013

Grasshoff, M., M. Erhardt, and K. Kremling. 1999. Methods of seawater analysis. Wiley-VCH. doi:10.1002/ange.19770890738

Guo, L., and P. H. Santschi. 2000. Sedimentary sources of old high molecular weight dissolved organic carbon from the ocean margin benthic nepheloid layer. Geochim. Cosmochim. Acta **64**: 651–660. https://linkinghub.elsevier.com/retrieve/pii/S001670379900335X

Haley, B. A., J. Du, A. N. Abbott, and J. McManus. 2017. The impact of benthic processes on rare earth element and neodymium isotope distributions in the oceans. Front. Mar. Sci. **4**: 1–12. doi:10.3389/fmars.2017.00426/full

Hansen, H., H. C. Giesenhagen, and G. Behrends. 1999. Seasonal and long-term control of bottom-water oxygen deficiency in a stratified shallow-water coastal system. ICES J. Mar. Sci. **56**: 65–71. doi:10.1006/jmsc.1999.0629

Heller, M. I., P. J. Lam, J. W. Moffett, C. P. Till, J. M. Lee, B. M. Toner, and M. A. Marcus. 2017. Accumulation of Fe oxyhydroxides in the Peruvian oxygen deficient zone implies non-oxygen dependent Fe oxidation. Geochim. Cosmochim. Acta **211**: 174–193. doi:10.1016/j.gca.2017.05.019

Holtappels, M., M. M. M. Kuypers, M. Schlüter, and V. Brüchert. 2011. Measurement and interpretation of solute concentration gradients in the benthic boundary layer. Limnol. Oceanogr.: Methods **9**: 1–13. doi:10.4319/lom.2011.9.1

Jacobs, L., S. Emerson, and J. Skei. 1985. Partitioning and transport of metals across the interface in a permanently anoxic basin: Framvaren Fjord, Norway. Geochim. Cosmochim. Acta **49**: 1433–1444. https://linkinghub.elsevier.com/retrieve/pii/0016703785902935

Koopmans, D., P. Berg, S. Brunner, and J. Val Klump. 2021. Seiche-and storm-driven benthic oxygen uptake in a eutrophic freshwater bay determined with aquatic eddy covariance. Freshw. Sci. **40**: 259–273. doi:10.1086/714542

Kremling, K., J. J. S. Tokos, L. Brügmann, and H. P. Hansen. 1997. Variability of dissolved and participate trace metals in the Kiel and Mecklenburg Bights of the Baltic Sea, 1990-1992. Mar. Pollut. Bull. **34**: 112–122.

von Langen, P. J., K. S. Johnson, K. H. Coale, and V. A. Elrod. 1997. Oxidation kinetics of manganese (II) in seawater at nanomolar concentrations. Geochim. Cosmochim. Acta **61**: 4945–4954.

Lennartz, S. T., A. Lehmann, J. Herrford, F. Malien, H. P. Hansen, H. Biester, and H. W. Bange. 2014. Long-term trends at the Boknis Eck time series station (Baltic Sea), 1957-2013: Does climate change counteract the decline in eutrophication? Biogeosciences **11**: 6323–6339.

Li, Y.-H., and S. Gregory. 1974. Diffusion of ions in sea water and in deep-sea sediments. Geochim. Cosmochim. Acta **38**: 703–714. http://www.scielo.br/scielo.php?script=sci_arttext&pid=S1414-98932014000401014&lng=pt&tlng=pt

Little, S. H., D. Vance, T. W. Lyons, and J. McManus. 2015. Controls on trace metal authigenic enrichment in reducing sediments: Insights from modern oxygen-deficient settings. Am. J. Sci. **315**: 77–119. doi:10.2475/02.2015.01

Lohan, M. C., and A. Tagliabue. 2018. Oceanic micronutrients: Trace metals that are essential for marine life. Elements **14**: 385–390. https://pubs.geoscienceworld.org/msa/elements/article/14/6/385/567322/Oceanic-Micronutrients-Trace-Metals-that-are

Millero, F. J., S. Sotolongo, and M. Izaguirre. 1987. The oxidation kinetics of Fe(II) in seawater. Geochim. Cosmochim. Acta **51**: 793–801. http://linkinghub.elsevier.com/retrieve/pii/0016703787900937

Moore, C. M., and others. 2013. Processes and patterns of oceanic nutrient limitation. Nat. Geosci. **6**: 701–710. doi:10.1038/ngeo1765

Morel, F. M. M. 2003. The biogeochemical cycles of trace metals in the oceans. Science (80-) **300**: 944–947. doi:10.1126/science.1083545

Morel, F. M. M., A. J. Milligan, and M. A. Saito. 2014. Marine bioinorganic chemistry: The role of trace metals in the oceanic cycles of major nutrients, p. 123–150. *In* Treatise on geochemistry. Elsevier. https://linkinghub.elsevier.com/retrieve/pii/B9780080959757006057

Morford, J. L., and S. Emerson. 1999. The geochemistry of redox sensitive trace metals in sediments. Geochim. Cosmochim. Acta **63**: 1735–1750. https://linkinghub.elsevier.com/retrieve/pii/S001670379900126X

Noble, A. E., and others. 2012. Basin-scale inputs of cobalt, iron, and manganese from the Benguela-Angola front

to the South Atlantic Ocean. Limnol. Oceanogr. **57**: 989–1010.

Oakey, N. S. 1982. Determination of the rate of dissipation of turbulent energy from simultaneous temperature and velocity shear microstructure measurements. J. Phys. Oceanogr. **12**: 256–271.

Osborn, T. R. 1980. Estimates of the local rate of vertical diffusion from dissipation measurements. J. Phys. Oceanogr. **10**: 83–89.

Pakhomova, S. V., P. O. J. Hall, M. Y. Kononets, A. G. Rozanov, A. Tengberg, and A. V. Vershinin. 2007. Fluxes of iron and manganese across the sediment–water interface under various redox conditions. Mar. Chem. **107**: 319–331. https://linkinghub.elsevier.com/retrieve/pii/S0304420307001302

Planquette, H., and R. M. Sherrell. 2012. Sampling for particulate trace element determination using water sampling bottles: Methodology and comparison to in situ pumps. Limnol. Oceanogr.: Methods **10**: 367–388. doi:10.4319/lom.2012.10.367

Plass, A., A. W. Dale, and F. Scholz. 2021. Sedimentary cycling and benthic fluxes of manganese, cobalt, nickel, copper, zinc and cadmium in the Peruvian oxygen minimum zone. Mar. Chem. **233**: 103982. https://linkinghub.elsevier.com/retrieve/pii/S0304420321000670

Plass, A., C. Schlosser, S. Sommer, A. W. Dale, E. P. Achterberg, and F. Scholz. 2020. The control of hydrogen sulfide on benthic iron and cadmium fluxes in the oxygen minimum zone off Peru. Biogeosciences **17**: 3685–3704. https://www.biogeosciences.net/17/3685/2020/

Pohl, C., and U. Hennings. 2005. The coupling of long-term trace metal trends to internal trace metal fluxes at the oxic–anoxic interface in the Gotland Basin (57°19,20′N; 20°03,00′E) Baltic Sea. J. Mar. Syst. **56**: 207–225. https://linkinghub.elsevier.com/retrieve/pii/S0924796304003033

Rapp, I., C. Schlosser, T. J. Browning, F. Wolf, F. A. C. Le Moigne, M. Gledhill, and E. P. Achterberg. 2020. El Niño-driven oxygenation impacts Peruvian shelf iron supply to the south Pacific Ocean. Geophys. Res. Lett. **47**(7): e2019GL086631. doi:10.1029/2019GL086631

Rapp, I., C. Schlosser, D. Rusiecka, M. Gledhill, and E. P. Achterberg. 2017. Automated preconcentration of Fe, Zn, Cu, Ni, Cd, Pb, Co, and Mn in seawater with analysis using high-resolution sector field inductively-coupled plasma mass spectrometry. Anal. Chim. Acta **976**: 1–13. doi:10.1016/j.aca.2017.05.008

Rapp, I., and others. 2019. Controls on redox-sensitive trace metals in the Mauritanian oxygen minimum zone. Biogeosciences **16**: 4157–4182. https://www.biogeosciences.net/16/4157/2019/

Reimers, C. E., and K. E. Fogaren. 2021. Bottom boundary layer oxygen fluxes during winter on the Oregon shelf. J. Geophys. Res. Oceans **126**: e2020JC016828. doi:10.1029/2020JC016828

Rickard, D. 2006. The solubility of FeS. Geochim. Cosmochim. Acta **70**: 5779–5789.

Rickard, D., and J. W. Morse. 2005. Acid volatile sulfide (AVS). Mar. Chem. **97**: 141–197.

Rigaud, S., O. Radakovitch, R. M. Couture, B. Deflandre, D. Cossa, C. Garnier, and J. M. Garnier. 2013. Mobility and fluxes of trace elements and nutrients at the sediment-water interface of a lagoon under contrasting water column oxygenation conditions. Appl. Geochem. **31**: 35–51. doi:10.1016/j.apgeochem.2012.12.003

Saito, M. A., T. J. Goepfert, and J. T. Ritt. 2008. Some thoughts on the concept of colimitation: Three definitions and the importance of bioavailability. Limnol. Oceanogr. **53**: 276–290. doi:10.4319/lo.2008.53.1.0276

Schlosser, C., P. Streu, M. Frank, G. Lavik, P. L. Croot, M. Dengler, and E. P. Achterberg. 2018. H_2S events in the Peruvian oxygen minimum zone facilitate enhanced dissolved Fe concentrations. Sci. Rep. **8**: 12642. http://www.nature.com/articles/s41598-018-30580-w

Scholz, F. 2018. Identifying oxygen minimum zone-type biogeochemical cycling in earth history using inorganic geochemical proxies. Earth-Sci. Rev. **184**: 29–45.

Scholz, F., C. Hensen, A. Noffke, A. Rohde, V. Liebetrau, and K. Wallmann. 2011. Early diagenesis of redox-sensitive trace metals in the Peru upwelling area - response to ENSO-related oxygen fluctuations in the water column. Geochim. Cosmochim. Acta **75**: 7257–7276. doi:10.1016/j.gca.2011.08.007

Scholz, F., J. Mcmanus, A. C. Mix, C. Hensen, and R. R. Schneider. 2014. The impact of ocean deoxygenation on iron release from continental margin sediments. Nat. Geosci. **7**: 433–437.

Scholz, F., and T. Neumann. 2007. Trace element diagenesis in pyrite-rich sediments of the Achterwasser lagoon, SW Baltic Sea. Mar. Chem. **107**: 516–532. https://linkinghub.elsevier.com/retrieve/pii/S030442030700196X

Scholz, F., and others. 2016. Nitrate-dependent iron oxidation limits iron transport in anoxic ocean regions. Earth Planet. Sci. Lett. **454**: 272–281. doi:10.1016/j.epsl.2016.09.025

Scor Working Group. 2007. GEOTRACES – an international study of the global marine biogeochemical cycles of trace elements and their isotopes. Geochemistry **67**: 85–131. https://linkinghub.elsevier.com/retrieve/pii/S0009281907000050

Smetacek, V. 1980. Annual cycle of sedimentation in relation to plankton ecology in western Kiel Bight. Ophelia (Suppl. 1): 65–76. https://oceanrep.geomar.de/21587/

Sundby, B., L. G. Anderson, P. O. J. Hall, Å. Iverfeldt, M. M. R. van der Loeff, and S. F. G. Westerlund. 1986. The effect of oxygen on release and uptake of cobalt, manganese, iron and phosphate at the sediment-water interface. Geochim. Cosmochim. Acta **50**: 1281–1288. https://linkinghub.elsevier.com/retrieve/pii/0016703786904114

Sundby, B., and N. Silverberg. 1985. Manganese fluxes in the benthic boundary layer 1. Limnol. Oceanogr. **30**: 372–381. doi:10.4319/lo.1985.30.2.0372

Sweere, T., S. van den Boorn, A. J. Dickson, and G.-J. Reichart. 2016. Definition of new trace-metal proxies for the controls on organic matter enrichment in marine sediments based on Mn, Co, Mo and Cd concentrations. Chem. Geol. **441**: 235–245. doi:10.1016/j.chemgeo.2016.08.028

Tribovillard, N., T. J. Algeo, T. Lyons, and A. Riboulleau. 2006. Trace metals as paleoredox and paleoproductivity proxies: An update. Chem. Geol. **232**: 12–32. https://linkinghub.elsevier.com/retrieve/pii/S000925410600132X

Acknowledgments

We would like to thank A. Petersen for crafting the Benthic Trace Profiler as well as our colleagues D. Jasinski, C. Schlosser, M. Schmidt, T. Steffens, and R. Surberg for technical and analytical assistance. We also thank the crew of RV *Alkor* for their support during the fieldwork. Three reviewers and the associated editor G. Cutter helped us to improve the manuscript. This study was supported by the German Research Foundation through the Emmy Noether Nachwuchsforschergruppe ICONOX (Iron Cycling in Continental Margin Sediments and the Nutrient and Oxygen Balance of the Ocean). Open access funding enabled and organized by Projekt DEAL.

Submitted 06 May 2021
Revised 15 September 2021
Accepted 30 November 2021

Associate editor: Gregory A. Cutter